Solution Structure of Kti11p from *Saccharomyces cerevisiae* Reveals a Novel Zinc-Binding Module[†,‡]

Jianping Sun,[§] Jiahai Zhang,[§] Fangming Wu,[§] Chao Xu,[§] Shujun Li,[||] Wei Zhao,[§] Ziyu Wu,[||] Jihui Wu,[§] Cong-Zhao Zhou,*[,§] and Yunyu Shi*[,§]

National Laboratory for Physical Sciences at Microscale and School of Life Sciences, University of Science and Technology of China, Hefei, Anhui, 230026, People's Republic of China, and Beijing Synchrotron Radiation Facility, Institute of High Energy Physics, Chinese Academy of Sciences, Beijing, 100039, People's Republic of China

Received March 14, 2005; Revised Manuscript Received April 26, 2005

ABSTRACT: Kti11p is a small, highly conserved CSL zinc finger-containing protein found in many eukaryotes. It was first identified as one of the factors required for maintaining the sensitivity of *Saccharomyces cerevisiae* to *Kluyveromyces lactis* zymocin. Then, it was found to be identical to Dph3, a protein required for diphthamide biosynthesis on eEF-2, the target of diphtheria toxin and *Pseudomonas* exotoxin A, in both yeast and higher eukaryotes. Furthermore, Kti11p/Dph3 was found to physically interact with core-Elongator, ribosomal proteins, eEF-2, two other proteins required for diphthamide modification on eEF-2, and DelGEF. Here, we determined the solution structure of Kti11p using NMR, providing the first structure of the CSL-class zinc-binding protein family. We present the first experimental evidence that Kti11p can bind a single Zn^{2+} ion by its four conserved cysteine residues. The major structure of Kti11p comprises a β sandwich as well as an α helix. Moreover, a structure-based similarity search suggests that it represents a novel structure and may define a new family of the zinc ribbon fold group. Therefore, our work provides a molecular basis for further understanding the multiple functions of Kti11p/Dph3 in different biological processes.

The zymocin, secreted by *Kluyveromyces lactis* killer strains to inhibit cellular growth of various sensitive yeast genera by a G1 cell cycle arrest in limited resources, is a plasmid-encoded three-subunit ($\alpha\beta\gamma$) bacterial toxin complex (*1*, *2*, *3*, *4*). Among the three subunits, the smallest one, the γ toxin, alone is vital for toxicity, and its conditional expression is enough to mimic the arrest (*5*). However, the α subunit, an exochitinase, and the β subunit are required for zymocin docking to cell-wall chitin and importing the γ toxin into cells to act with the targets (*6*, *7*).

Recent work has demonstrated that the *K. lactis* zymocin model of action is linked to RNA polymerase II function via Elongator (*8*). TOT,[1] the putative *K. lactis* γ-toxin target complex from *Saccharomyces cerevisiae*, has been characterized (*8*, *9*). TOT is encoded by *TOT1*−*7*, six loci of which are isoallelic to RNA polymerase II (RNAP II) Elongator genes (*ELP1*−*6*) and mutations in which result in *tot* phenotype, including zymocin resistance, thermosensitivity, slow growth, a G1 cell-cycle delay, and hypersensitivity to the drugs (*8*−*13*). The holo-Elongator contains the core complex (Elp1−3p) and the HAP complex (histone acetyltransferase-associated proteins) (Elp4−6p) (*10*−*12*, *14*, *15*). Core-Elongator binds stably to the elongating form of RNAP II (*15*). Elp1p was found to be involved in maintaining the structural integrity of Elongator (*15*). Elp3p/TOT3p has histone acetyltransferase (HAT) activity, and this activity is essential for both zymocin sensitivity (*9*, *10*) and Elongator function *in vivo*, which most probably creates a chromatin environment to facilitate the efficient transcription by RNAP II (*11*, *16*).

Kti11p is a small protein found in many eukaryotes. It was first identified as one of the factors required for conferring sensitivity of *S. cerevisiae* to *K. lactis* zymocin (*17*, *18*). Disruption or mutagenesis of *KTI11* resulted in *tot* phenotype, including zymocin resistance (*18*). Combining disruption in *KTI11* with a deletion in *TOT3*/*ELP3*, which yielded synthetic effects on slow growth phenotype expression, suggests that *KTI11* interacts genetically with *TOT3* and is possibly linked to the TOT/Elongator function (*18*).

[†] This work was supported by the Chinese National Fundamental Research Project (Grants G1999075605 and 2002CB713806), the Chinese National Natural Science Foundation (Grants 30270293, 30121001, and 30470366), the Key Project of the National High Technology Research and Development Program of China (Grant 2002BA711A13), the Pilot Project of the Knowledge Innovation Program of the Chinese Academy of Science (Grant KSCX1-SW-17), and the 100-talent project from Chinese Academy of Science.

[‡] The atomic coordinates have been deposited in the RCSB Protein Data Bank (accession code 1YOP).

* To whom correspondence should be addressed. Telephone: 86-551-3607464. Fax: 86-551-3601443. E-mail: yyshi@ustc.edu.cn (Y.S.) or zcz@ustc.edu.cn (C.-Z.Z.).

[§] University of Science and Technology of China.

[||] Chinese Academy of Sciences.

[1] Abbreviations: eEF-2, eukaryote translation elongation factor 2; TOT, γ-toxin target; DelGEF, deafness locus-associated guanine nucleotide exchange factor; IPTG, isopropyl β-D-thiogalactopyranoside; 2D and 3D, two and three dimensional; NMR, nuclear magnetic resonance; HSQC, heteronuclear single-quantum correlation; NOE, nuclear Overhauser effect; NOESY, nuclear Overhauser effect spectroscopy; TOCSY, total correlated spectroscopy; rmsd, root-mean-square deviation; EXAFS, extracted X-ray absorption extended fine structure.

10.1021/bi0504714 CCC: $30.25
Published on Web 05/25/2005

This is reinforced by the evidence that Kti11p can protect the N terminal of Elongator subunit Elp1p/Tot1p from post-translational modification/proteolysis (*19*).

Dph3, the analogue of Kti11pin Chinese hamster ovary (CHO) cell, required for the first step of diphthamide synthesis in the post-translational modification of translation elongation factor 2 (eEF-2) at His715, was identified recently (*20*). Diphthamide is the target of bacterial ADP-ribosylating toxin DT (Diphtheria toxin) and ETA (*Pseudomonas* exotoxin A). There are five genes (*DPH 1*−*5*) involved in the first step of diphthamide synthesis (*22*). Interestingly, the loss of *DPH1* and *DPH2* suppressed zymocicity, which suggests a possibility that Dph1 and Dph2 may be linked to TOT/Elongator or vice versa via Kti11p/Dph3 (*19*).

Recently, Kti11p was found to interact with many different proteins. Using tandem affinity purification analysis, Kti11p was found to associate with core-Elongator (Elp1p−Elp3p), translation proteins (Rps7Ap and Rps19Ap), eEF-2, and proteins involved in diphthamide synthesis (Dph1 and Dph2). The association of Kti11p/Dph3 with Dph1 and Dph2 suggests the existance of a catalytic protein complex to participate in the diphthamide synthesis (*21*). In addition, DelGIP1, the homologue of Kti11p in humans (shared 39% amino acid identity), was characterized to interact with DelGEF, which is a putative deafness locus-associated guanine nucleotide exchange factor (*23*, *24*). Kti11p and its homologues when taken together may play multiple roles in the regulation of transcription, translation elongation, zymocicity, diphtheria toxicity, and even DelGEF and most likely serve as an interactor involved in protein−protein interactions in different protein complexes.

Using the conserved domain architecture retrieval tool (CDART), we performed sequence similarity searches of Kti11p against the NCBI Protein Database based on conserved domain architecture. It was found that Kti11p belongs to a highly conserved CSL zinc finger-containing protein family in eukaryotes from yeast to humans. However, despite the extensive studies on the roles of Kti11p, up to date, we have very little knowledge about the structural basis of this CSL-class zinc-binding protein family. To further our knowledge about the precise roles of Kti11p/Dph3 and to better understand the possible function for other proteins in this family, we determined the solution structure of Kti11p in zinc-binding forms by NMR, which represents the first structure of this family. Structure-based similarity search suggests that it has a novel structure and may define a new family of the zinc ribbon fold group in the zinc fingers database (http://prodata.swmed.edu/zndb/) (*25*). Moreover, we provided the first experimental evidence that Kti11p can coordinate a single zinc ion by its four conserved cysteine residues. Therefore, our work opened new perspectives to understand not only the mechanism of Kti11p/Dph3 in Elongator complex TOT function, zymocicity, and other biological processes but also the possible function of the correlated CSL zinc-binding proteins.

EXPERIMENTAL PROCEDURES

Cloning, Expression, and Purification of Kti11p. The complete open-reading frame of *KTI11* (YBL071W-A) from *S. cerevisiae* S288C was cloned into a pET28a+ expression vector (Novagen) to give an N-terminal methionine followed by a valine and a 6× His tag at its C terminus. The recombinant plasmid was then transformed to *Escherichia coli* BL21 (DE3) Gold (Stratagene) host cells and incubated at 37 °C until $A_{600} = 1.0$ in M9 medium. Expression was induced by adding 1 mM IPTG and 20 uM $ZnSO_4$ at 16 °C for 20 h. Uniformly labeled recombinant Kti11p was produced using M9 medium containing 0.5 g/L 99% ^{15}N ammonium sulfate and 2.5 g/L 99% ^{13}C-glucose as the sole nitrogen and carbon source, respectively

Kti11p was purified using a Nickel-Chelating Sepharose Fast Flow (Amersham Pharmacia Biotech) followed by gel filtration in a HiLoad 16/60 Superdex 75 with an HPLC system (Amersham Pharmacia Biotech). The purity of Kti11p was confirmed by SDS−PAGE, and the protein concentration was measured with BCA kits (Pierce). The ^{15}N-labeled and ^{13}C,^{15}N-labeled Kti11p was about 0.6−0.8 mM. All of the samples for the NMR study contain 20 mM Tris buffer (pH 7.0) and 50 mM NaCl in 90% H_2O/10% D_2O or 99.9% D_2O.

EXAFS Spectroscopy. The protein sample was prepared, as mentioned above, using M9 medium with limited zinc resource for EXAFS (extracted X-ray absorption extended fine structure) analysis.

The EXAFSs at the K edge of zinc-Kti11p sample were collected in "fluorescence yield" (FY) mode using a Si(111) double crystal monochromator, at the X-ray absorption station (beam line 1W1B) of Beijing Synchrotron Radiation Facility (BSRF). The storage ring was operating at the typical energy of 2.2 GeV, with the current decreasing approximately from 135 to 80 mA during a time span of 8 h. To suppress unwanted harmonics, a detuning of 30% was performed between the two crystals of the monochromator. The incident beam intensity was monitored and recorded using ionization chamber filled by 25% argon-doped nitrogen mixture, and the fluorescence signal was collected and recorded by a fluorescence ionization chamber filled by argon gas.

EXAFS analyses were performed by the code WinXAS (version 3.1) (*26*) through fitting the EXAFS oscillation with the theoretical models, which were generated using Feff 7.0 (*27*). Because sulfur atom has much stronger backscattering ability than carbon or nitrogen atoms do, almost all of the EXAFS signal was contributed by four nearest first-shell sulfur atoms. We fitted the spectra corresponding to the first shell, which consists of four sulfur atoms only, both in momentum space (k space) and real space (R space) for the Zn spectrum. During the fitting, the coordination number was always fixed at 4, whereas the average coordination distance R, scale factor S_0^2, Debye−Waller factor σ^2, and E_0 shift were all allowed to vary.

NMR Spectroscopy and Data Processing. All NMR experiments were performed at 298 K on a Bruker DMX600 spectrometer with self-shielded *z*-axis gradients. Backbone and side-chain resonances were assigned using the following experiments: 2D ^1H, ^{15}N-HSQC, 2D ^1H, ^{13}C-HSQC, 3D triple-resonance spectra HNCO, HN(CA)CO, CBCA(CO)-NH, CBCANH, C(CO)NH-TOCSY, H(CCO)NH-TOCSY ^{15}N-TOCSY, HCCH-TOCSY, HCCH-COSY, HBHA(CB-CACO)NH, and 2D CB(CC)HD-COSY (aromatics). NMR distance information was obtained from three different NOESY spectra: 3D NOESY−^{15}N-HSQC (mixing time 100 ms) in water for amide protons, 3D NOESY−^{13}C-HSQC (mixing time 130 ms) in water for aliphatic protons, and 2D

^{1}H-NOESY in D_2O (mixing time 100 ms) for aromatic protons. The ^{15}N-labeled sample was lyophilized and dissolved in 99.96% D_2O, used in the H/D-exchange experiment, to get hydrogen-bond restraints.

NMR data processing was carried out using NMRPipe and NMRDraw software, and the data were analyzed with PIPP. Linear prediction (*28*) was used to improve spectral resolution in the indirect dimensions where constant-time acquisition was used, for example, the ^{15}N evolution dimension in all of the triple-resonance experiments mentioned above.

Structure Calculation. The NOE distance restraints obtained from different NOESY spectra, as mentioned above, were classified into four categories: strong (1.8−3.0 Å), medium (1.8−4.0 Å), weak (1.8−5.0 Å), and very weak (1.8−6.0 Å). The 1.8 Å lower limits were imposed only implicitly by the van der Waals repulsion force. Considering that the spin diffusion effect could be serious for aliphatic and aromatic protons, a more conservative distance estimation was used for the latter two NOESY; therefore, most medium- and long-range NOEs from these two spectra were put into the weak or very weak groups, while most intraresidue NOEs were not used. For methyl protons, nonstereospecifically assigned methylene protons, and aromatic ring protons, r^{-6} summation averages were applied (*29*).

Backbone dihedral angle restraints were obtained from chemical-shift index (CSI) (*30*). The CSI was calculated for four types of nuclear: Cα, Cβ, C′, and Hα. The derived secondary structures based on the consensus CSI were converted into restraints on Φ and Ψ angles: for α-helix residues, Φ was limited in $-60 \pm 40°$ while Ψ was in $-50 \pm 50°$; for β-strand residues, Φ was limited in $-120 \pm 40°$ while Ψ was in $130 \pm 50°$. Hydrogen-bond restraints were obtained by identifying the slow-exchange amide protons located in regular secondary structures, displaying characteristic NOE cross-peaks. Each deduced hydrogen bond was represented by two distance constraints: α-helix residues, 1.6−2.4 Å for H^N−O and 2.4−3.3 Å for N−O; β-strand residues, 1.4−2.7 Å for H^N−O and 2.4−3.7 Å for N−O.

Structures were calculated using the program CNS version 1.1 (*31*) using the experimentally derived restraints (1101 NOEs, 51 dihedral angle restraints, and 54 hydrogen bonds). Initial rounds of refinement used only NOE data and dihedral angle restraints, which defined the general fold of the domain and revealed the stereochemistry about the coordinated zinc. Final refinements added four EXAFS-derived restraints for zinc-S_γ (2.30−2.33 Å) and six idealized restraints for S_γ−S_γ distances (3.60−3.90 Å) to ensure approximate tetrahedral zinc coordination as well as hydrogen-bond restraints. Structures were analyzed and displayed using PROCHECK-NMR (*32*) and MOLMOL (*33*).

RESULTS AND DISCUSSION

Kti11p Is a Zinc-Binding Module. Kti11p is encoded by the ORF YBL071W-A from *S. cerevisiae*. The sequences of Kti11p homologues from various eukaryotic organisms are highly conserved, and we found that many highly conserved residues are distributed throughout almost the whole protein. These conserved residues can be divided into three classes: four cysteine residues (class I, marked with ● in Figure 1A); hydrophilic residues with negative charge (class II, marked with ▲ in Figure 1A); and other residues (class III), most of which are hydrophobic. The Pfam and NCBI protein database suggest *KTI11* encodes a CSL zinc-binding (pfam05207) protein, which is named after its conserved motif of the final cysteine. The four conserved cysteine residues (Cys 26, 28, 48, and 51) are thought to be potential zinc-binding ligands.

Kti11p was expressed in *E. coli* using M9 medium with limited zinc resource, and the soluble protein was purified to homogeneity under nondenaturing conditions (see the Experimental Procedures). As expected, the presence of a single zinc ion was demonstrated by using atomic absorption spectroscopy (0.83 mol of zinc/mol of Kti11p).

In addition, as an ideal technique to define the local structure around a metal ion inside of the protein, the EXAFS spectrum was used here. The initial structural model was taken from our preliminary structure, which is calculated by using the NMR experimentally derived restraints (1101 NOEs and 51 dihedral angle restraints). According to the initial structure calculation, besides four sulfur atoms from the four conserved cysteines around the zinc ion inside Kit11p, the other possibility involves four nitrogen atoms from the C-terminal 6 His tags. Thus, we tested whether zinc chelated through four nitrogen atoms or four sulfur atoms by EXAFS. As shown in parts B and C of Figure 1, only the experimental data coincided with the given model (sulfur atoms around the zinc ion inside Kit11p) very well, while the fitting results are very unreasonable when using four nitrogen atoms around the zinc ion as an initial model (data not shown), on the basis of a fixed coordination number of 4 during fitting.

Usually, the most efficient EXAFS analyses are based on the Fourier transformation of the data expressed in momentum space (k space) to real space (R space). The absolute value of the transform is found to peak at distances shifted from the real values by several tenths angstroms because of the shift phase. Therefore, as shown in Figure 1C, the position of the Fourier transformation peak indicates an apparent distance as about 2.0 Å. The real distance from the absorption atom Zn^{2+} to coordination sulfur atoms is the sum of a apparent distance and the phase shift [here, the phase shift is calculated by feff 7.0 (*27, 34*) and is about 0.31 Å]. Therefore, the EXAFS analyses revealed that the Zn^{2+} coordinates to four sulfur atoms with an average Zn−S bond length of 2.31 Å. Furthermore, the Debye−Waller factors σ^2 are 0.006 53 Å, suggesting a slightly distorted tetrahedral geometry about the zinc ion center (*35*). Thus, we conclude that Kti11p contains a $Zn(Cys)_4$ motif and coordinates a single, tetrahedral Zn^{2+} ion using its four conserved cysteine residues.

NMR Studies of Kti11p. Kti11p is a small protein of only 82 residues and contains a single glutamine, two asparagines, and seven prolines. Under low-salt conditions, a well-resolved 2D ^{1}H-^{15}N HSQC spectrum of Kti11p was obtained at 25 °C with 71 expected correlation peaks for the backbone amide proton and 6 peaks for asparagine and glutamine side-chain amide protons resolved (Figure 2). In this spectrum, cross-peaks for M1, V2, and A81−83 were not observed (M1 and V2 come from vector pET28a+).

Using standard ^{1}H/^{13}C/^{15}N heteronuclear NMR experiments mentioned in experiments, we obtained nearly complete resonance and stereospecific assignments for Kti11p

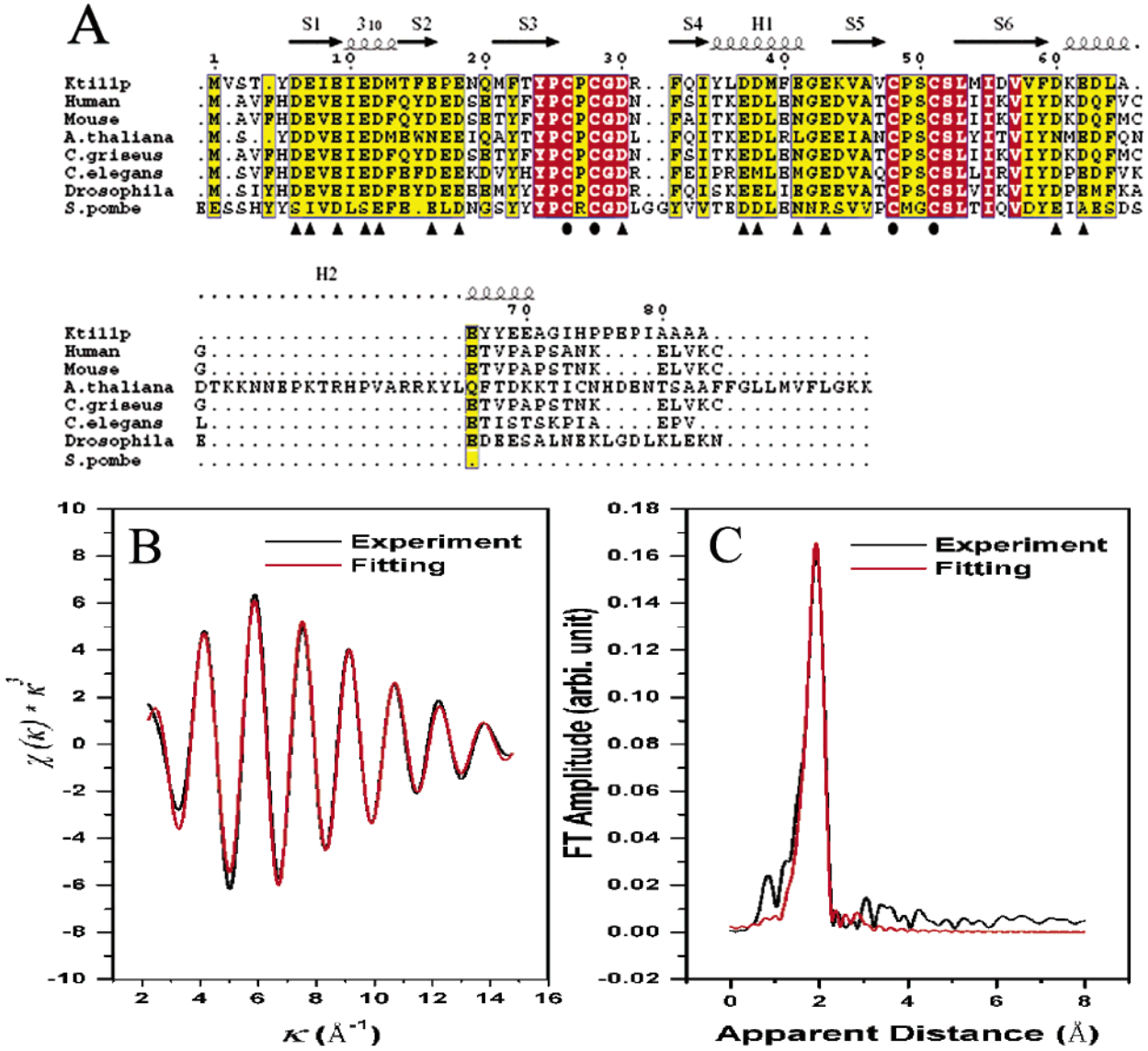

FIGURE 1: Sequence alignments of Kti11p homologues and EXAFS fitting results in κ space and R space for Kti11p. (A) Protein sequences were from *Saccharomyces cerevisiae* (Kti11p, database accession no NP_660100), *Homo sapiens* (human, NP_996662), *Mus musculus* (mouse, AAH39954), *Arabidopsis thaliana* (*A. thaliana*, AAD41975), *Cricetulus griseus* (*C. griseus*, AAQ83755) *Caenorhabditis elegans* (*C. elegan*, AAQ83755), *Drosophila melanogaster* (*Drosophila*, NP_650057), and *Schizosaccharomyces pombe* (*S. pombe*, NP_594366). The secondary structure of Kti11p is indicated above the alignment. The identical residues in the alignment are shown in red boxes; those similar are shown in yellow boxes. The elucidations for these markers: ●, conserved cysteines involved in metal binding; ▲, conserved hydrophilic amino acids with negative charges. Residue Val2 of Kti11p comes from the expression vector. **(**B) EXAFS spectrum in κ space with a black line for the experiment curve and a red line for the best fitted theoretical model. (C) EXAFS spectrum in R space with a black line for the experiment curve and a red line for the best fitted theoretical model as well.

with the exception of Pro75 and C-terminal residues (81−83). As expected for a $Zn(Cys)_4$ metal center, the four cysteine C_β resonances exhibited chemical shifts (29.5−31.8 ppm) that were intermediate between free cysteine (28.3 ppm) and oxidized cysteine (41.2 ppm).

The structure determination of Kti11p was based on a total of 1216 restraints comprising 1101 interproton distance constraints, 54 distance restraints for hydrogen bonds, 51 dihedral angle restraints, and 10 distance restraints for tetrahedral zinc coordination (4 experimental and 6 idealized restraints). A total of 100 accepted structures were calculated, and structural statistics for the 20 lowest energy structures, which had no NOE violations larger than 0.2 Å and no dihedral angle violations greater than 5°, are summarized in Table 1. In the selected 20 structures, 77.5% of the residues were in the most favored region on the Ramachandran plot using PROCHECK (32), 20.8% in the additionally allowed region, 1.2% in the generously allowed region, and 0.5% in the disallowed region. Unlike the well-structured region (residues 5−70), the N- and C-terminal regions (residues 1−4 and 71−83) are disordered. Root-mean-square deviation (rmsd) values in the structured region versus the mean coordinates are 0.50 Å for the backbone atoms and 1.06 Å for all heavy atoms. Figure 2A shows the superposition of the family of 20 selected structures.

Overall Structure of Kti11p. The structure of Kti11p folds into a closed, compact, and globular protein structure, which comprises a zinc ion, a 3_{10} helix, two turns, two α helices (H1 and H2), and two β sheets (Figure 2B). The two β sheets are composed of strands S1 (residues 6−9), S5 (residues 44−47), and S6 (residues 53−59) for the first sheet and strands S2 (residues 14−16), S3 (residues 21−24), and S4 (residues

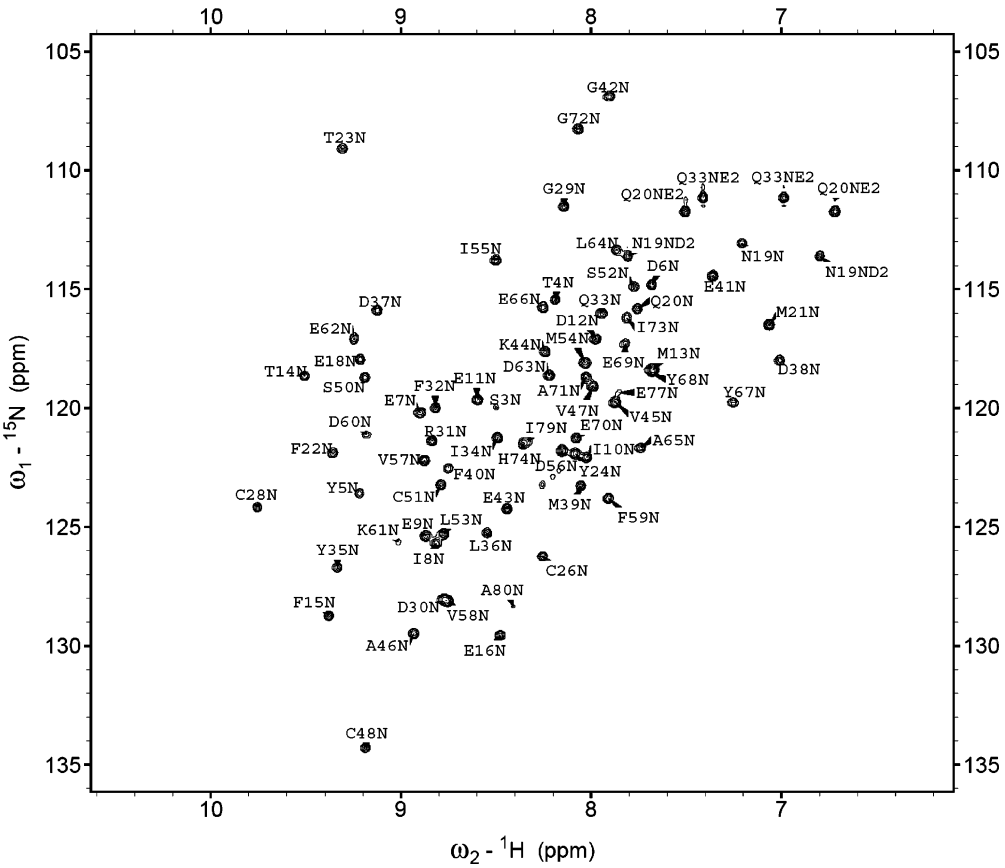

FIGURE 2: ^{1}H-^{15}N HSQC spectra of ^{15}N-labeled Kti11p at 600 MHz and 25 °C. Conditions: 20 mM Tris buffer (pH 7.0) and 50 mM NaCl in 90% H_2O/10% D_2O. Sequential assignments are indicated adjacent to each peak.

Table 1: Structural Statistics for the Family of 20 Structures[a]

distance restraints	
intraresidue ($i - j = 0$)	320
sequential ($\|i - j\| = 1$)	356
medium range ($2 < \| i - j\| < 4$)	156
long range ($\| i - j\| > 5$)	279
hydrogen bonds	54
dihedral angle restraints	51
total	1216
mean rmsd values from	
the experimental restraints	
distance	0.0049 ± 0.0001
dihedral	0.0085 ± 0.0073
mean rmsd values from	
idealized covalent geometry	
bonds (Å)	0.0008 ± 0.00003
angles (deg)	0.2609 ± 0.0013
impropers (deg)	0.0866 ± 0.0018
Ramachandran plot[b] (%)	
residues in most favorable regions	77.5
residues in additional allowed regions	20.8
residues in generously allowed regions	1.2
residues in disallowed regions	0.5
atomic rms differences[c] (residues 5−70)[d] (Å)	
backbone heavy atom (N, C^{α},and C′)	0.501
heavy atoms	1.062

[a] None of the structure exhibits distance violations greater than 0.2 Å or dihedral angle violations greater than 5°. [b] Procheck was used to assess the overall quality of the structures [c] The precision of the atomic coordinates is defined as the average rms difference between the 20 final structures and the mean coordinates of the protein. Superposition and overall rmsd values were calculated using MOLMOL. [d] The unstructured portions of the N- and C-terminal tails were not considered.

32−34) for another sheet. Moreover, the two β sheets, separated by the 3_{10} helix and the shorter helix H1 (residues 36−40), face each other face to form a $\beta-\alpha-\beta$ sandwich structure. Between the strands S1 and S3, there is a larger groove, and a smaller groove is formed by S4, S5, and helix H1. The zinc-binding site is at the top of the β sandwich, which is contributed by the two turns, usually called knuckles. The four cysteine residues, coordinated Zn^{2+}, lie in the two knuckles protruding from the two β hairpins (S3−S4 and S5−S6). The entrance of the β sandwich is closed by the longer α-helix H2.

The core domain of Kti11p is further stabilized by a network of hydrophobic interactions among side chains of the well-conserved residues such as Ile8, Ile10, Met13, Phe22, Phe32, Leu36, Met39, Ile55, and Val57 (Figure 1A and Figure 2C). These highly hydrophobic residues lie in the cavity of the β sandwich and contribute to the stability of the zinc-binding motif and the whole structure. Notably, the hydrophobic sides of the two helices almost in parallel are also facing the hydrophobic cavity, like a lid of the β sandwich, to form a hydrophobic core.

In addition, judging from the structure, the zinc cluster environment includes two NH−O hydrogen bonds, C26CO−G29NH and L53CO−C48NH, and four NH−S_{γ} hydrogen bonds, C48S_{γ}−S50NH, C48S_{γ}−C51NH, C26S_{γ}−C28NH, and C28S_{γ}−D30NH. These hydrogen bonds are consistent with the H−D exchange experiments, and this network contributes to the stabilization of the coordination of the zinc ion. Interestingly, we also found that, around the cluster, all oxygen atoms of the carboxyl groups are extensively located on the surface of the zinc-binding site and form electrical dipoles with several NH atoms (Figure 2D). This arrangement usually exists in many zinc fingers, such as TFIIS (1TFI) (36), zinc-substituted rubredoxin (1DX8 and 1IRN)

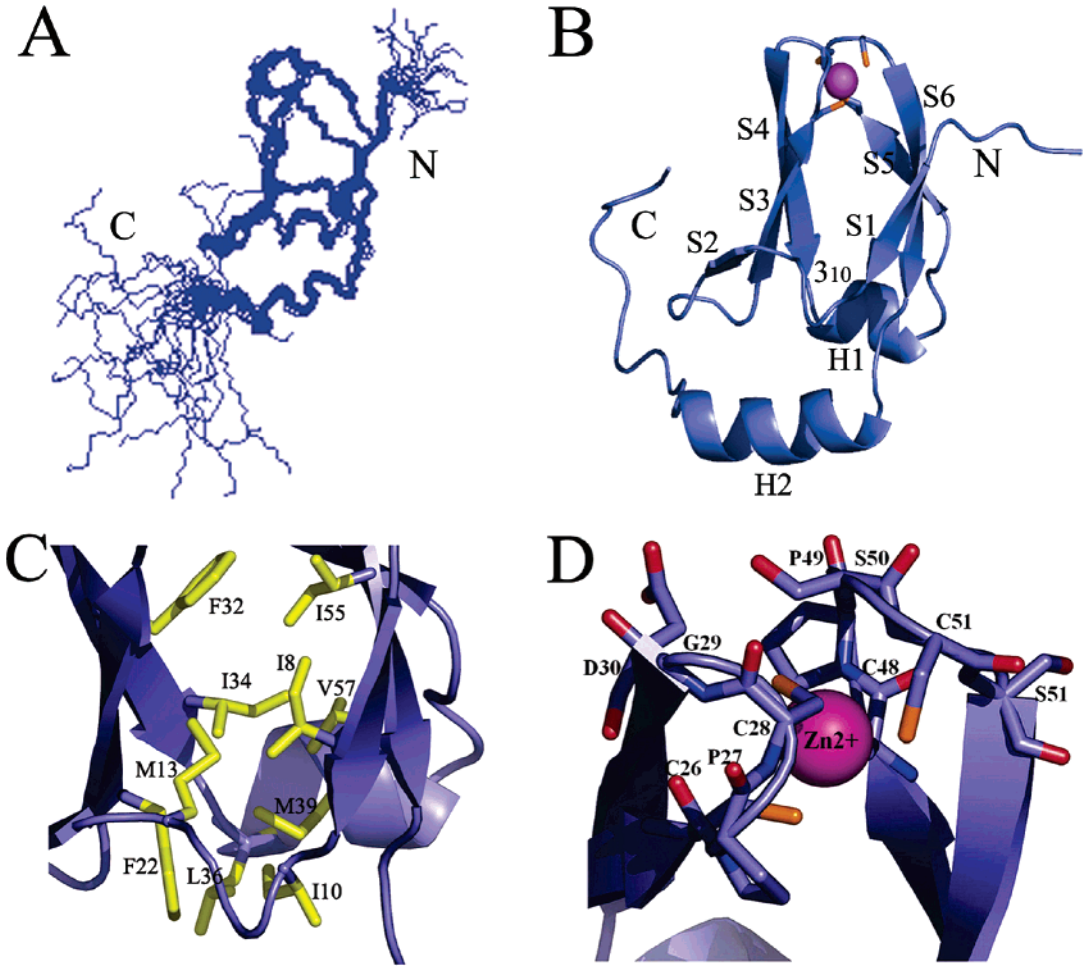

FIGURE 3: NMR structure of Kti11p. (A) Backbone superposition of 20 selected structures from the final CNS calculation. (B) Ribbon representation of the minimized average structure (zinc ion is shown as purple spheres). Cysteines coordinate to zinc are shown by a stick. (C) Hydrophobic core. The hydrophobic residues are shown by a stick and colored yellow. (D) Surface of the zinc-binding site. All oxygen atoms are colored red. The figure was produced with MOLMOL and PyMOL.

(*37*), and ribosomal protein L36 (1DFE) (*38*), which is possibly favored to balance the negative charges around the zinc ion and stabilize the motif.

Kti11p is a small acidic protein of only 82 residues with a theoretical pI of 3.56. As described previously, Kti11p possesses a high percentage of conserved negatively charged residues (14 of 82 residues, marked with ▲ in Figure 1A). These residues are located at the surface of the β sandwich and forming two rather largely negatively charged electrostatic potential surfaces (shown in Figure 3). On the lager surface, there are mainly seven conserved electronegative residues including Asp6, Glu7, Glu9, Glu11, Asp12, Glu16, and Glu18 (Figure 3A), almost all of which lie in the first three β strands. The smaller potential binding surface opposite to the lager surface is formed by residues Asp37, Asp38, Glu41, and Glu43 (Figure 3B), three of which are located at the shorter helix H1. These conserved residues may play similar roles in different organisms.

Kti11p Defines a Novel Family of the Zinc Ribbon Fold Group. Searching for a similar structure of Kti11p using DALI (*39*) (http://www.ebi.ac.uk/dali/), we failed to identify very close structural homologues, except for two hits with very low *Z* scores of 1.8 (PDB code 1l3a-A and rmsd = 4.1 Å for 61 residues) and 1.4 (PDB code 1d5r-A and rmsd = 3.0 Å for 50 residues). During detailed analysis, no significant match was obtained from the superimposition of Kti11p on the two candidates. Generally, a *Z* score < 2.0 typically indicates a structurally dissimilar pair; thus, we suggest that Kti11p contains a novel structure.

In addition, the sequence similarity search of Kti11p against the NCBI Protein Database by using the conserved domain architecture retrieval tool (CDART) reveals 57 hits, most of which are hypothetical or unknown proteins, containing a CSL zinc finger domain. These proteins are classified into two families: one composes of two tandem domains started with a DnaJ domain at the N terminus, and the other composes a single CSL zinc finger domain, such as Kti11p. Remarkably, none of them has been structurally characterized; thus, our research gave the first structure of this protein family.

Because Kti11p contains a zinc-binding motif, we performed a comparison with all known zinc finger structures in the zinc fingers database (*25*). On the basis of the structural properties in the vicinity of the zinc-binding site, currently available zinc finger structures are classified into 8-fold groups, and the structures within each group are further classified into families based on the hypothesized homology among the proteins in the same family (*25*).

According to their definitions, the structure of Kti11p is clearly classified into the zinc ribbon fold group, because it possesses two knuckles in the zinc-binding site (*25*). The zinc ribbon fold group contains nine families, including

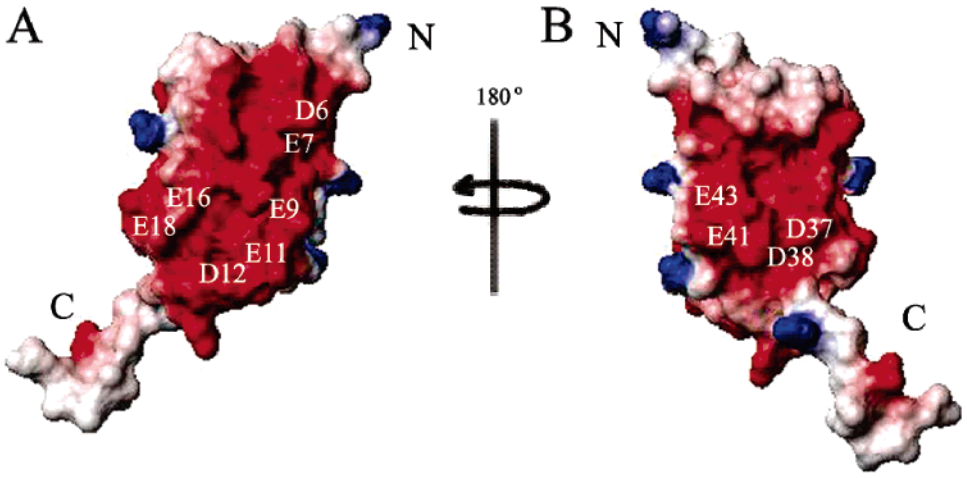

FIGURE 4: Surface distributions of conserved electronegative residues and electrostatic potential surfaces of Kti11p. (A) Electrostatic potential surface of Kti11p is colored red for electronegative residues and blue for electropositive residues. (B) Rotated 180° from A about a vertical axis in the plane of the paper. All conserved negatively charged residues are mapped onto the surface colored by white numbers. The figure was prepared by MOLMOL.

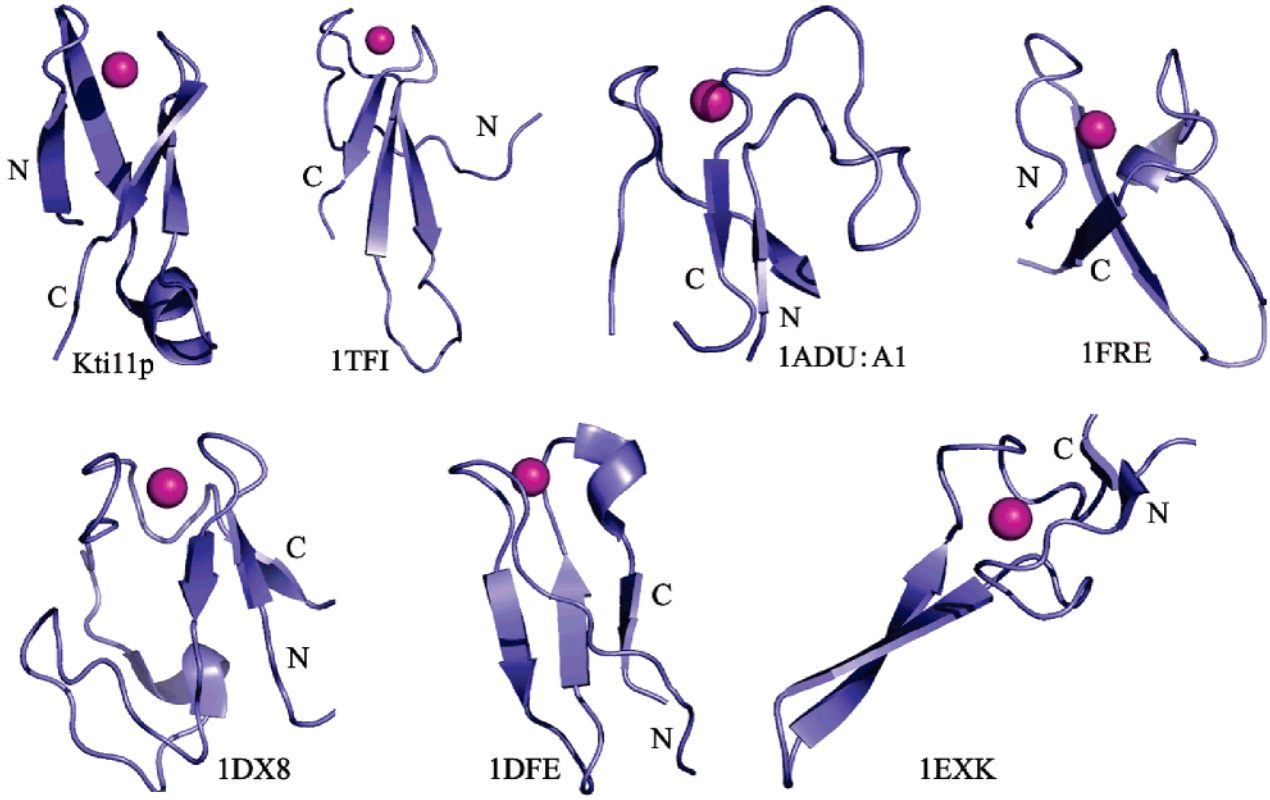

FIGURE 5: Structural comparison of Kti11p with the representative of some families in the zinc-ribbon fold group. Zinc ribbons from Kti11p (PDB code 1YOP), classical zinc ribbon (1TFI), the AdDBP zinc ribbons (1ADU, A1), the B-box zinc finger (1FRE), rubredoxin family (1DX8), ribosomal protein L36 (1DFE), and the cysteine-rich domain of the chaperone protein DnaJ (1EXK, A2) are shown to illustrate the difference in orientation and topology. Zinc ions are shown as spheres.

classic zinc ribbons, the cluster-binding domain of rieske iron sulfur protein, the adenovirus DNA-binding protein zinc ribbons, the B-box zinc finger, rubredoxin family, rubredoxin-like domains in enzymes, btk motif, ribosomal protein L36, and the cysteine-rich domain of the chaperone protein DnaJ.

We comprehensively compared the structure of Kti11p with the representative member of some families in the zinc ribbon fold group (Figure 5), which Kti11p may be classified into. However, Kti11p holds an entirely different structure from these selected representative zinc ribbon domains. Architectures of the zinc-binding sites of these proteins (Kti11p; TFIIS, 1TFI; and zinc-substituted rubredoxin, 1DX8) (*36*, *38*) are similar to each other. However, despite the similar knuckles and inter-zinc distances, the structure of Kti11p is quite different from any of them either in topology or in structural conservation. For instance, the topology of TFIIS (*36*), the B-box zinc finger (1FRE) (*40*), rubredoxin family (1DX8) (*38*), and ribosomal protein L36 (1DFE) (*41*) are $\beta\beta\beta$, $\beta\alpha\beta$, $\beta\beta\alpha\beta$, and $\beta\beta\alpha\beta$, respectively, which form the zinc-binding subsites, whereas the topology of Kti11p is different as $\beta\beta\alpha\beta\beta$, forming two β sheets separated by a short α helix. As for the structural conservation, most of the zinc ribbons frequently display limited

sequence similarity restricted to the zinc ligands and the zinc knuckle motifs (*25*), whereas the structure of Kti11p shares little similarity with other zinc-binding domains except for the geometry of zinc ligands and conserved cysteines. According to their definitions that the structures within 1-fold should be grouped into one family based on the hypothesized homology (*25*), Kti11p and its homologies are proposed to define a new family within the zinc ribbon fold group.

CONCLUSIONS

In recent years, the importance of Kti11p in elongator function, zymocicity, transcription regulation, and translation diphtheria toxicity has been increasingly recognized. It is involved in a lot of protein−protein interactions. The structure determination of Kti11p provides the first structural template for the CSL zinc finger domain containing protein family. We showed that Kti11p defines a novel structure and may fall into a new family in the zinc ribbon fold group. Our work provides a structural basis for further systematic biochemical, genetic, and microbiological studies aimed at understanding the multiple functions of Kti11p/Dph3 in different biological processes and at elucidating the functions of other CSL zinc-binding proteins.

ACKNOWLEDGMENT

We thank Dr. J. Mackay, especially Dr. A. Kwan, and Dr. S. Alam for their kind help in structural calculation. We also thank Dr. F. Delaglio and Dr. A. Bax for providing the software NMRPipe, Dr. T. D. Goddard and Dr. D. G. Kneller for providing Sparky, and Dr. L. D. Warren for providing PyMOL.

REFERENCES

1. Stark, M. J. R., Boyd, A., Mileham, A. J., and Romanos, M. A. (1990) The plasmid-encoded killer system of *Kluyveromyces lactis*: A review, *Yeast 6*, 1−29.
2. Butler, A. R., White, J. H., and Stark, M. J. (1991) Analysis of the response of *Saccharomyces cerevisiae* cells to *Kluyveromyces lactis* toxin, *J. Gen. Microbiol. 137*, 1749−17573.
3. Schaffrath, R., and Breunig, K. D. (2000) Genetics and molecular physiology of the yeast *Kluyveromyces lactis*, *Fungal Genet. Biol. 30*, 173−190.
4. Meinhardt, F., and Schaffrath, R. (2001) Extranuclear inheritance: Cytoplasmic linear double-stranded DNA killer elements of the dairy yeast *Kluyveromyces lactis*, *Prog. Bot. 62*, 51−70.
5. Butler, A. R., Porter, M., and Stark, M. J. (1991) Intracellular expression of *Kluyveromyces lactis* toxin γ subunit mimics treatment with exogenous toxin and distinguishes two classes of toxin-resistant mutant, *Yeast 7*, 617−625.
6. Butler, A. R., O'Donnell, R. W., Martin, V. J., Gooday, G. W., and Stark, M. J. (1991) *Kluyveromyces lactis* toxin has an essential chitinase activity, *Eur. J. Biochem. 199*, 483−488.
7. Jablonowski, D., Fichtner, L., Martin, V. J., Klassen, R., Meinhardt, F., Stark, M. J. R., and Schaffrath, R. (2001) *Saccharomyces cerevisiae* cell wall chitin, the *Kluyveromyces lactis* zymocin receptor, *Yeast 18*, 1285−1299.
8. Jablonowski, D., Frohloff, F., Fichtner, L., Stark, M. J. R., and Schaffrath, R. (2001) *Kluyveromyces lactis* zymocin mode of action is linked to RNA polymerase II function via Elongator, *Mol. Microbiol. 42*, 1095−1106.
9. Frohloff, F., Fichtner, L., Jablonowski, D., Breunig, K. D., and Schaffrath, R. (2001) *Saccharomyces cerevisiae* Elongator mutations confer resistance to the *Kluyveromyces lactis* zymocin, *EMBO J. 20*, 1993−2003.
10. Winkler, G. S., Petrakis, T. G., Ethelberg, S., Tokunaga, M., Erdjument-Bromage, H., Tempst, P., and Svejstrup, J. Q. (2001) RNA polymerase II elongator holoenzyme is composed of two discrete subcomplexes, *J. Biol. Chem. 276*, 32743−32749.
11. Otero, G., Fellows, J., Li, Y., de Bizemont, T., Dirac, A. M., Gustafsson, C. M., et al. (1999) Elongator, a multisubunit component of a novel RNA polymerase II holoenzyme for transcriptional elongation, *Mol. Cell* 3, 109−118.
12. Wittschieben, B. O., Otero, G., de Bizemont, T., Fellows, J., Erdjument-Bromage, H., Ohba, R., et al. (1999) A novel histone acetyltransferase is an integral subunit of elongating RNA polymerase II holoenzyme, *Mol. Cell 4*, 123−128.
13. Fellows, J., Erdjument-Bromage, H., Tempst, P., and Svejstrup, J. Q. (2000) The Elp2 subunit of elongator and elongating RNA polymerase II holoenzyme is a WD40 repeat protein, *J. Biol. Chem. 275*, 12896−12899.
14. Krogan, N. J., and Greenblatt, J. F. (2001) Characterization of a six-subunit holo-Elongator complex required for the regulated expression of a group of genes in *Saccharomyces cerevisiae*, *Mol. Cell Biol. 21*, 8203−8212.
15. Li, Y., Takagi, Y., Jiang, Y., Tokunaga, M., Erdjument-Bromage, H., Tempst, P., and Kornberg, R. D. (2001) A multiprotein complex that interacts with RNA polymerase II Elongator, *J. Biol. Chem. 276*, 29628−29631.
16. Wittschieben, B. O., Du Fellows, J. W., Stillman, D. J., and Svejstrup, J. Q. (2000) Overlapping roles for the histone acetyltransferase activities of SAGA and elongator *in vivo*, *EMBO J. 19*, 3060−3068.
17. Butler, A. R., White, J. H., Folawiyo, Y., Edlin, A., Gardiner, D., and Stark, M. J. R. (1994) Two *Saccharomyces cerevisiae* genes which control sensitivity to G1 arrest induced by *Kluyveromyces lactis* toxin, *Mol. Cell Biol. 14*, 6306−6316.
18. Fichtner, L., and Schaffrath, R. (2002) *KTI11* and *KTI13*, *Saccharomyces cerevisiae* genes controlling sensitivity to G1 arrest induced by *Kluyveromyces lactis* zymocin, *Mol. Microbiol. 44*, 865−875.
19. Fichtner, L., Jablonowski, D., Schierhorn, A., Kitamoto, H. K., Stark, M. J., and Schaffrath, R. (2003) Elongator's toxin-target (TOT) function is nuclear localization sequence dependent and suppressed by post-translational modification, *Mol. Microbiol. 49*, 1297−1307.
20. Liu, S., and Leppla, S. H. (2003) Retroviral insertional mutagenesis identifies a small protein required for synthesis of diphthamide, the target of bacterial ADP-ribosylating toxins, *Mol. Cell 12*, 603−613.
21. Liu, S., Milne, G. T., Kuremsky, J. G., Fink, G. R., Leppla, S. H. (2004) Identification of the proteins required for biosynthesis of diphthamide, the target of bacterial ADP-ribosylating toxins on translation elongation factor 2, *Mol. Cell Biol. 24*, 9487−9497.
22. Corda, D., and Di Girolamo, M. (2003) Functional aspects of protein mono-ADP-ribosylation, *EMBO J. 22*, 1953−1958.
23. Sjolinder, M., Uhlmann, J., and Ponstingl, H. (2002) DelGEF, a homologue of the Ran guanine nucleotide exchange factor RanGEF, binds to the exocyst component Sec5 and modulates secretion, *FEBS Lett. 532*, 211−215.
24. Sjolinder, M., Uhlmann, J., and Ponstingl, H. (2004) Characterization of an evolutionary conserved protein interacting with the putative guanine nucleotide exchange factor DelGEF and modulating secretion, *Exp. Cell Res. 294*, 68−76.
25. Krishna, S. S., Majumdar, I., and Grishin, N. V. (2003) Survey and summary structural classification of zinc fingers, *Nucleic Acids Res. 31*, 532−550.
26. Ressler, T., Brock, S. L., Wong, J., and Suib, S. L. (1999) Multiple-scattering EXAFS analysis of tetraalkylammonium manganese oxide colloids, *J. Phys. Chem. B 103*, 6407−6420.
27. Ankudinov, A. L., and Rehr, J. J. (1997) Relativistic calculations of spin-dependent X-ray-absorption spectra, *Phys. Rev. B: Condens. Matter Mater. Phys. 56*, 1712−1716.
28. Barkhuijsen, H., de Beer, R., Bovee, W. M., Creyghton, J. H., and van Ormondt, D. (1985) Application of linear prediction and singular value decomposition (LPSVD) to determine NMR frequencies and intensities from the FID, *Magn. Reson. Med. 2*, 86−89.
29. Nilges, M. (1993) A calculation strategy for the structure determination of symmetric dimers by ^{1}H NMR, *Proteins 17*, 297−309.
30. Wishart, D. S., and Sykes, B. D. (1994) The ^{13}C chemical-shift index: A simple method for the identification of protein secondary structure using ^{13}C chemical-shift data, *J. Biomol. NMR 4*, 171−180.
31. Brunger, A. T., Adams, P. D., Clore, G. M., Delano, W. L., Gros, P., Grosse-Kunstleve, R. W., Jiang, J.-S., Kuszewski, J., Nilges, M., Pannu, N. S., Read, R. J., Rice, L. M., Simonson, T., and

Warren, G. L. (1998) Crystallography and NMR system: A new software suite for macromolecular structure determination, *Acta Crystallogr., Sect. D 54*, 905−921.
32. Laskowski, R. A., Rullmann, J. A., MacArthur, M. W., Kaptein, R., and Thornton, J. M. (1996) AQUA and PROCHECK-NMR: Programs for checking the quality of protein structure solved by NMR, *J. Biomol. NMR 8*, 477−486.
33. Koradi, R., Billeter, M., and Wüthrich, K. (1996) MOLMOL: A program for display and analysis of macromolecular structures, *J. Mol. Graphics 14*, 51−55.
34. Feiters, M. C., Eijkelenboom, A. P. A. M., Nolting, H.-F., Krebs, B., van den Ent, F. M. I., Plasterk, R. H. A., Kaptein, R., and Boelens, R. (2003) X-ray absorption spectroscopic studies of zinc in the N-terminal domain of HIV-2 integrase and model compounds, *J. Synchrotron Radiat. 10*, 86−95.
35. Wang, B., Alam, S. L., Meyer, H. H., Payne, M., Stemmler, T. L., Davis, D. R., Sundquist, W. I. (2003) Structure and ubiquitin interactions of the conserved zinc finger domain of Npl4, *J. Biol. Chem. 278*, 20225−20234.
36. Qian, X., Gozani, S. N., Yoon, H., Jeon, C. J., Agarwal, K., and Weiss, M. A. (1993) Novel zinc finger motif in the basal transcriptional machinery: Three-dimensional NMR studies of the nucleic acid binding domain of transcriptional elongation factor TFIIS, *Biochemistry 32*, 9944−9959.
37. Schweimer, K., Hoffmann, S., Wastl, J., Maier, U. G., Rosch, P., Sticht, H. (2000) Solution structure of a zinc substituted eukaryotic rubredoxin from the cryptomonad alga guillardia theta, *Protein Sci. 9*, 1474−1486.
38. Hard, T., Rak, A., Allard, P., Kloo, L., and Garber, M. (2000) The solution structure of ribosomal protein L36 from *Thermus thermophilus* reveals a zinc-ribbon-like fold, *J. Mol. Biol. 296*, 169−180.
39. Holm, L., and Sander, C. (1993) Protein structure comparison by alignment of distance matrices, *J. Mol. Biol. 233*, 123−138.
40. Borden, K. L., Lally, J. M., Martin, S. R., O'Reilly, N. J., Etkin, L. D., and Freemont, P. S. (1995) Novel topology of a zinc-binding domain from a protein involved in regulating early *Xenopus* development, *EMBO J. 14*, 5947−5956.
41. Hard, T., Rak, A., Allard, P., Kloo, L., and Garber, M. (2000) The solution structure of ribosomal protein L36 from *Thermus thermophilus* reveals a zinc-ribbon-like fold, *J. Mol. Biol. 296*, 169−180.

BI0504714